

Dynamics of Dewetting

C. Redon, F. Brochard-Wyart, and F. Rondelez

*Laboratoire de Structure et Reactivité aux Interfaces, Université Pierre et Marie Curie,
11 rue Pierre et Marie Curie, 75231 Paris CEDEX 05, France*

(Received 15 October 1990)

Films of silicone oils (or alkanes) deposited on low-energy surfaces (grafted silicon wafers) are metastable. We nucleate a dry spot at the center of the wafer and observe the rate of growth $V = dR/dt$ of the dry patch of radius R . We find that V is (a) independent of R , (b) independent of the film thickness, (c) inversely proportional to the oil viscosity, and (d) very sensitive to the value of θ_e , the equilibrium contact angle between oil and wafer. At small θ_e , $V \approx \theta_e^3$. All these features are in agreement with a recent hydrodynamic theory.

PACS numbers: 68.15.+e, 47.20.-k, 62.15.+i

The spontaneous spreading of nonvolatile liquids on ideal wettable solid surfaces is relatively well understood.¹⁻⁴ In the present experiments, we study for the first time the inverse process, where the solid is not wettable but a liquid film (of typical thickness 20 μm) has been forced onto the surface. For these macroscopic films, the long-range van der Waals forces are negligible and the plot of the free energy F versus the thickness e in a horizontal geometry is controlled by weak gravitational forces (Fig. 1). All films below a certain thickness e_c (≈ 1 mm) are metastable.^{5,6} They evolve by nucleation and growth of dry patches. These dewetting processes (which can often be seen qualitatively on a windshield or

in a bathtub) are of importance in many engineering problems: In some cases (e.g., greenhouses) the aim is to maintain such a film and avoid droplet formation, whereas in other cases (e.g., windscreens) the film must be eliminated rapidly (to avoid frost formation).

On the fundamental side, there is an interesting similarity between Fig. 1, which shows the possibility of an equilibrium between a dry and a wet solid, and phase-separation processes. In our case, however, the dynamics is controlled by macroscopic hydrodynamic flows.⁷ Moreover, this work has a usefulness beyond the drying mechanisms: It relates to other hydrodynamic problems such as the draining and formation of dark spots in soap films.⁸

We have used two different liquid-solid pairs to produce nonwettable surfaces: (a) alkanes on aliphatic chains and (b) silicone oils on perfluorinated chains.

In both cases, the chains were grafted onto the SiO_2 surface of a silicon wafer⁹ using octadecyltrichlorosilane in case (a) and heptadecafluoro 1,1,2,2-tetrahydrodecyltrichlorosilane in case (b). Following Zisman,¹⁰ contact-angle measurements against a series of alkanes gave critical surface tensions $\gamma_c^{(a)} = 21 \pm 2$ mN m^{-1} and $\gamma_c^{(b)} = 15 \pm 2$ mN m^{-1} , respectively. The alkanes used in our dewetting experiments (purchased from Merck) have surface tensions γ ranging from 21.8 to 27.6 mN m^{-1} . This allows strong variations in the equilibrium contact angle θ_e , given by $\gamma \cos \theta_e = \gamma_c$ in the limit of small θ_e (see Table I). On the other hand, the viscosity η of the different alkanes is nearly the same. By contrast, polydimethylsiloxane (PDMS) silicone oils, which can be purchased from Petrarch with different molecular weights, have nearly identical surface tension ($\gamma = 21.2$ – 21.5 mN m^{-1}) but their viscosity can be varied over several orders of magnitude by a suitable choice of the chain length.

PDMS films of uniform thickness e were prepared by spin coating. The thickness of the film (20–50 μm) was measured by weighing the wafers before and after deposition. With the low-viscosity alkanes, spin coating was not possible: The films were prepared instead by draw-

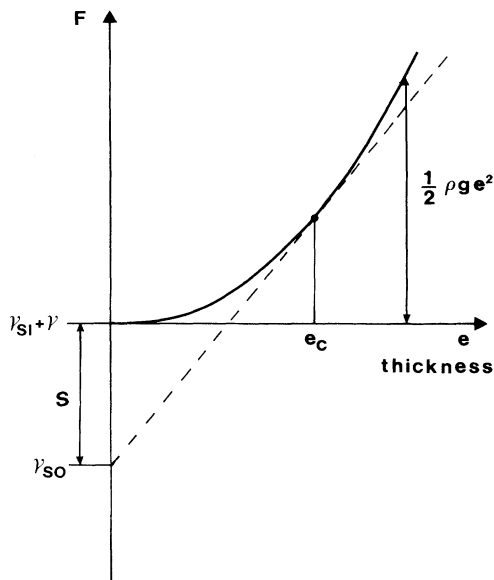


FIG. 1. Free energy per unit area F vs thickness e in the case of a solid wetted by a liquid film of thickness $e \approx 10$ – 1000 μm . F is controlled by interfacial and gravitational energies. γ_{so} , γ_{sl} , and γ are the solid-vapor, solid-liquid, and liquid-vapor interfacial tensions, respectively. The film is metastable at $e < e_c$ since $d^2F/de^2 > 0$ and evolves via nucleation and growth of a dry spot.

TABLE I. Physical parameters and dewetting velocities V for the alkanes and silicone oils. γ and η are the liquid surface tension and viscosity, respectively. $V^* = \gamma/\eta$ is the characteristic fluid velocity. L is the prefactor value required to fit Eq. (6). For PDMS, two qualities of fluorinated silicon wafers, referred by the number (1) or (2), respectively, have been used.

M_w	θ_a (deg)	θ_r (deg)	θ_e (deg)	γ (mNm ⁻¹)	η (mPas)	V^* (mm s ⁻¹)	V (μ m s ⁻¹)	L
PDMS								
5970 (1)	53.5	49.5	51.5	20.9	96.6	216	580	16
(2)	45.0	35.0	40.0				243	17.8
17250 (1)	54.0	50.0	52.0	21.1	485.5	43.5	113	16.9
28000 (1)	56.0	50.0	53.0	21.2	971	21.8	53.5	19
(2)	46.0	35.0	40.5				23	19.7
49350 (1)	58.0	50.0	54.0	21.3	4865	4.4	12.7	17.1
62700 (1)	60.0	50.0	55.0	21.5	11700	1.8	10	9.6
(1)	54.0	50.0	52.0				9	9.0
116500 (1)	60.0	50.0	55.0	21.5	58600	0.4	1.9	10
Alkanes								
Nonane			15.3	22.9	0.7	32200	6000	6.0
Decane			19.0	23.9	0.9	26000	9200	6.0
Dodecane	$\theta_a - \theta_r < 2^\circ$		22.0	25.4	1.4	18800	10000	6.3
Hexadecane			36.0	27.6	3.3	8300	19900	6.0

ing a wet paper across the wafer (a technique which is commonly used for cleaning laser mirrors).

Two different methods were used to create the initial hole: (i) capillary suction at the center of the fluid film with a glass capillary of diameter ≈ 1 mm and (ii) blowing a dry air jet perpendicular to the surface (for the most viscous liquids).

The evolution of the ruptured film at later times was monitored by a video camera: Each frame was acquired in 40 ms with a spatial resolution of 50 μ m. The dynamic contact angle θ_d around the dry spot was measured by an optical reflectivity method,¹¹ with an accuracy of 0.5° provided that the hole velocity was slow. This is especially true for the most viscous PDMS which have typical velocities in the μ m/s range. The same method was used to measure the static contact angle θ_e when $\theta_e < 40^\circ$. Larger angles ($\theta_e > 40^\circ$) were measured by projecting the image of a sessile droplet onto a screen in the far field. The accuracy was $\approx 3^\circ$ for $\theta_e \approx 50^\circ$. The difference between advancing θ_a and receding θ_r contact angles ranges between 1° for case (a) and 11° for case (b) (see Table I). Somewhat arbitrarily we took for θ_e the mean value $\theta_e = \frac{1}{2}(\theta_a + \theta_r)$. This procedure defines the equilibrium contact angle with an accuracy $\Delta\theta = \frac{1}{2} \times (\theta_a - \theta_r)$.

We now describe the mechanism of dewetting. Figure 2(a) shows a dry patch after nucleation of a hole (radius $R_0 \approx 1$ mm) in a liquid film of PDMS of molecular weight 28000. The hole appears circular at all times, except for a few defects pinning the contact line (dust particles or surface defects on the silicon wafer). The liquid removed from the dry path accumulates into a visible rim. The width of the rim increases with time and reaches 1 mm at the end of the experiment (11 min). Talc particles powdered on the liquid allow us to check

that the native film outside of the rim remains motionless. The mean radius $R(t)$ of the dry region is plotted in Fig. 2(b): The velocity $V = dR/dt$ is constant during the expansion (from 1 to 11 mm) and equals $V = 14$ μ m/s. The (receding) dynamic contact angle was found to be time independent: $\theta_d = 23.2^\circ \pm 0.2^\circ$ for this particular experiment. This value is markedly smaller than the static contact angle $\theta_e = 30^\circ \pm 2^\circ$ for a sessile droplet of the same PDMS deposited at equilibrium on the same substrate. Systematic measurements show a fixed ratio between these two angles:

$$\theta_d/\theta_e \approx 0.7 \pm 0.2. \quad (1)$$

Experiments on other liquids confirm that the hole always opens at *constant velocity* V in a broad range of velocities ranging from cm/s for the alkanes to cm/h for the PDMS of molecular weight 116500. Moreover, V is found to be independent of the initial thickness e of the film in the range $0.1e_c < e < 0.8e_c$, where the critical thickness e_c is related to the capillary length $\kappa^{-1} = (\gamma/\rho g)^{1/2}$ by $e_c = 2\kappa^{-1} \sin\theta_e/2$. (In our experiments, e_c varies from 0.5 to 1 mm for alkanes, while for PDMS e_c is about 1 mm.) A similar result has also been obtained by Petrov and Sedev by monitoring the motion of the contact line upon entrainment and drainage of glycerol-water films on hydrophobic substrates.¹²

We have then studied the role of the fluid viscosity η . By using PDMS films of four different molecular weights deposited on the same fluorinated substrate we obtain

$$V \approx \eta^{-1} \quad (2)$$

at fixed contact angle (see Fig. 3).

We have finally looked at the dependence of V upon the static contact angle θ_e by using four different alkanes on the same wafer (Table I). The results are plotted in

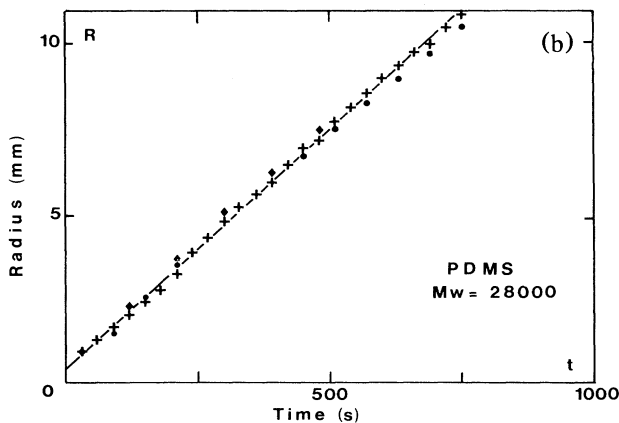
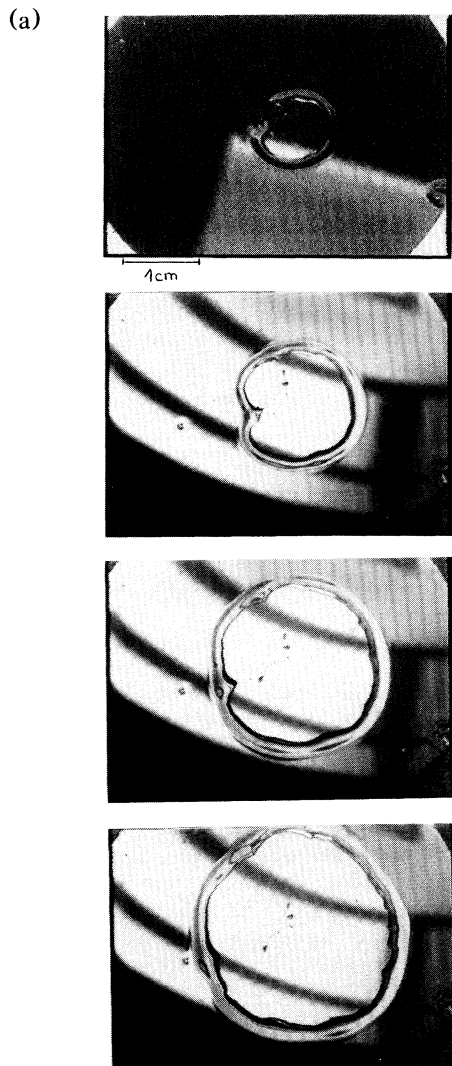


FIG. 2. (a) Snapshot of an expanding dry patch in a liquid film of PDMS of molecular weight 28 000 deposited on a fluorinated wafer. Full view size, 4 cm. Film thickness is 30 μm . (b) Time dependence of the mean radius R of the dry region. The different symbols (+, ●, ◆) correspond to three different radial directions away from the center.

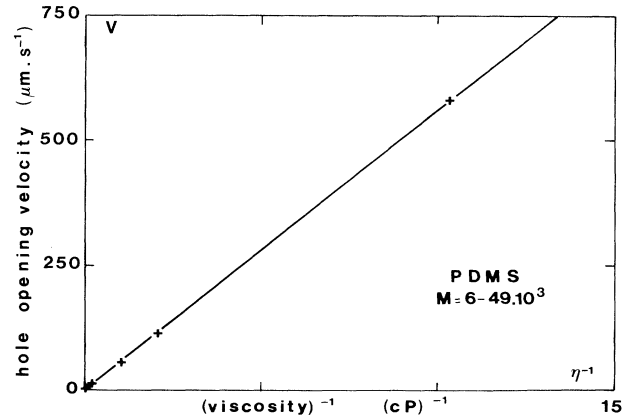


FIG. 3. Dewetting velocity V as a function of the inverse viscosity η^{-1} for PDMS silicone oils of various molecular weights.

Fig. 4 as the capillary number V/V^* (where $V^* = \gamma/\eta$) vs θ_e^3 . We observe that in the range $\theta_e = 15^\circ - 36^\circ$ all points fall on a straight line. Figure 4 also shows some results obtained with silicone oils of identical surface tension γ but deposited on silicon wafers with different surface treatments. There is again a linear dependence of V on θ_e^3 but the prefactor is clearly different between the low- and high-molecular-weight PDMS. It has to be noticed that the larger dispersion of the data for the PDMS samples is due to the contact-angle hysteresis on the fluorinated wafers. These whole series of experiments can be condensed in the simple equation

$$V/V^* = k\theta_e^3, \tag{3}$$

where k depends on the nature and on the molecular weight of the liquid.

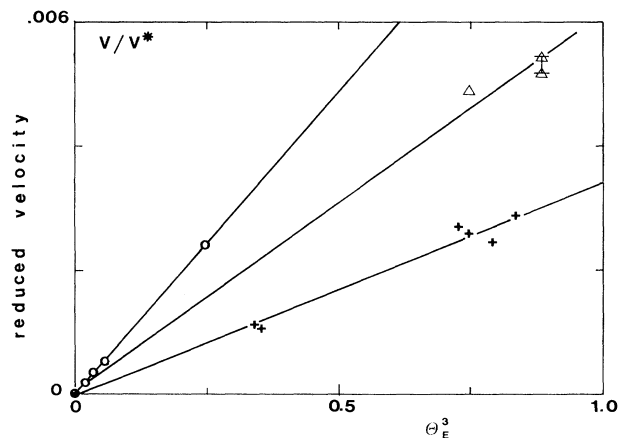


FIG. 4. Reduced velocity V/V^* as a function of the equilibrium contact angle θ_e for alkanes (○), low-molecular-weight PDMS ($M_w < 50000$) (+), and high-molecular-weight PDMS ($M_w > 50000$) (Δ). $V^* = \gamma/\eta$. From the slopes, the parameter L of Eq. (6) is found to be $L_\circ = 6$, $L_+ = 17$, $L_\Delta = 10$, respectively.

The important role played by surface tension and viscosity (through θ_e and V^* , respectively) in Eq. (3) suggests that drying is controlled by a competition between capillary forces and viscous flow. Based on this finding, we have compared our result with a recent hydrodynamic theory of drying (for films of thickness $e \ll e_c$) which is detailed in Refs. 7, 8, and 13. We briefly summarize the results here, following Ref. 1: After a dry patch has nucleated at some point on the solid, it will expand only if its size R_0 is larger than a threshold R_c .⁶ Then a rim appears ahead of the dry patch [Fig. 2(a)]. The rim cross section is a portion of a circle (with a dynamic contact angle θ_d) because the pressure is expected to equilibrate rapidly in the rim. The dynamical contact angle θ_d is related to the velocities V_A and V_B of the inner (*A*) and outer (*B*) contact lines which limit the rim. For small angles ($\theta_e, \theta_d \ll 1$), one has

$$\frac{1}{2} \gamma (\theta_e^2 - \theta_d^2) = 3\eta L \theta_d^{-1} V_A, \quad (4a)$$

$$\frac{1}{2} \gamma \theta_d^2 = 3\eta L \theta_d^{-1} V_B. \quad (4b)$$

The left-hand sides of Eqs. 4(a) and 4(b) represent the uncompensated Young force, while the right-hand sides describe the viscous force due to the flow in a wedge of angle θ_d . L is a logarithmic factor of order 10 and is due to the divergence of the dissipation in a wedge. As discussed in detail in Ref. 14, $L \approx \ln(la^{-1}\theta_d^2)$, where a is a microscopic cutoff length depending on the nature of the liquid and l is the width of the rim. In our experiments $l(t) \ll R(t)$ and thus $V_A \approx V_B = V$. Equations (4a) and (4b) then lead to

$$\theta_d = \theta_e / \sqrt{2}, \quad (5)$$

$$V/V^* = (1/12L\sqrt{2})\theta_e^3. \quad (6)$$

Both of these predictions are well confirmed by our data [Eqs. (1)–(3)]. Moreover, our experimental values of L , which range between 6 for the alkanes and 20 for the less viscous PDMS, are consistent with the generally agreed values. It should be remarked that the above description will no longer hold when the size of the rim l is larger than the capillary length $\kappa^{-1} \approx 1$ mm. Then the rim is flattened by gravitational forces, and the dissipation in the flat part becomes important.⁵

It appears from our results that dewetting proceeds by a transformation of interfacial energies into macroscopic viscous losses, at least in our condition of slow flows, $V/V^* \ll 1$. A different line of interpretation where the

dissipation is ascribed to molecular processes on the contact line¹⁵ is ruled out by our experiments. Indeed, the dewetting velocity $V \approx V^* \theta_e^3 \approx V^* \theta_d^3$ [Eqs. (1) and (3)] depends critically on the factor η/θ_d (in the limit of $\theta_d \ll 1$). This factor, first computed by Huh and Scriven,¹⁶ is specific of hydrodynamic losses in a thin wedge. On the other hand, the molecular losses may start to show up at higher velocities ($\theta_d \approx 1$), where the Huh-Scriven factor is smaller.

We thank J. B. Brozka and P. Silberzan for the preparation of grafted silicon wafers, P. G. de Gennes for numerous discussions on the theory of dewetting, and S. Troian for reading the manuscript. Laboratoire de Structure et Réactivité aux Interfaces is laboratoire associé au CNRS, URA No. 1319.

¹P. G. de Gennes, *Rev. Mod. Phys.* **57**, 827 (1985).

²J. Daillant, J. J. Bennatar, and L. Leger, *Phys. Rev. A* **41**, 1963 (1990).

³F. Heslot, N. Fraysse, and A. M. Cazabat, *Nature (London)* **338**, 640 (1989).

⁴J. D. Chen and N. Wada, *Phys. Rev. Lett.* **62**, 3050 (1988).

⁵F. Brochard-Wyart, C. Redon, and F. Rondelez, *C. R. Acad. Sci. (Paris), Ser. II* **306**, 1143 (1988).

⁶A. Sharma and E. Ruckenstein, *J. Colloid Interface Sci.* **133**, 358 (1989).

⁷F. Brochard-Wyart, J. M. di Meglio, and D. Quéré, *C. R. Acad. Sci. (Paris), Ser. II* **304**, 553 (1987).

⁸As pointed out by one of us in Ref. 7, there is a strong analogy between the growth of a dry patch on a wet surface and the growth of a black film region in a soap film, previously discussed by P. G. de Gennes, *C. R. Acad. Sci. (Paris), Ser. II* **303**, 1275 (1986).

⁹R. Maoz and J. Sagiv, *J. Colloid Interface Sci.* **100**, 465 (1984).

¹⁰W. A. Zisman, *Adv. Chem.* **43**, 1 (1964).

¹¹C. Allain, D. Ausseré, and F. Rondelez, *J. Colloid Interface Sci.* **107**, 5 (1985).

¹²J. G. Petrov and R. V. Sedev, *Colloids Surf.* **13**, 313 (1985).

¹³F. Brochard-Wyart and J. Daillant, *Can. J. Phys.* (to be published).

¹⁴P. G. de Gennes, X. Hua, and P. Levinson, *J. Fluid Mech.* **212**, 55 (1990).

¹⁵T. D. Blake and K. J. Ruschak, *Nature (London)* **282**, 489 (1979); T. D. Blake and J. M. Haynes, *J. Colloid Interface Sci.* **30**, 421 (1969).

¹⁶C. Huh and L. E. Scriven, *J. Colloid Interface Sci.* **35**, 85 (1971).

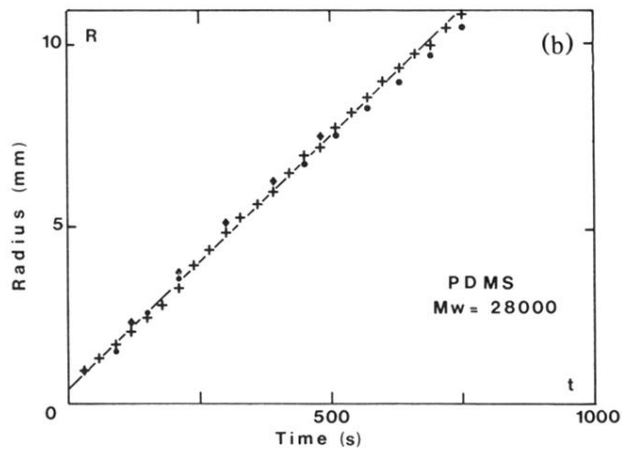
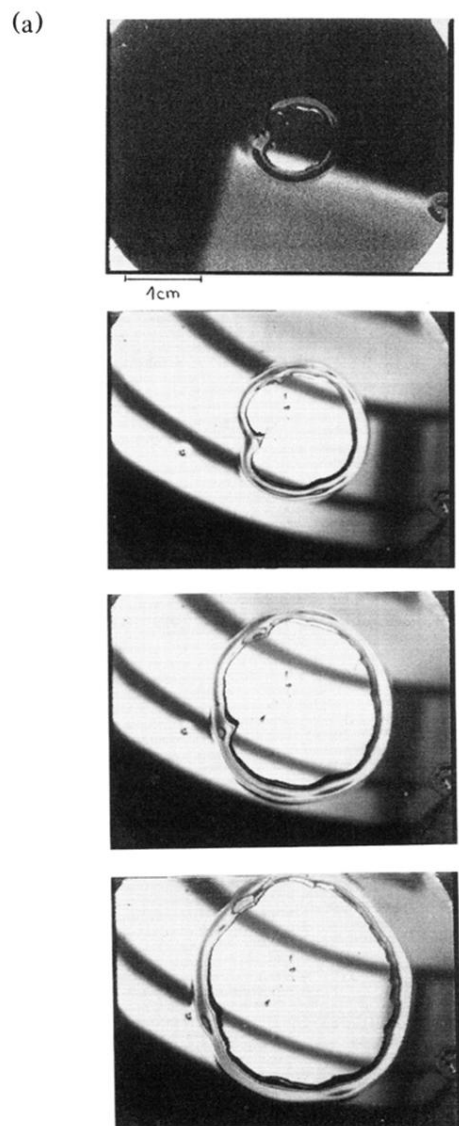


FIG. 2. (a) Snapshot of an expanding dry patch in a liquid film of PDMS of molecular weight 28 000 deposited on a fluorinated wafer. Full view size, 4 cm. Film thickness is $30 \mu\text{m}$. (b) Time dependence of the mean radius R of the dry region. The different symbols (+, ●, ◆) correspond to three different radial directions away from the center.